Journal of Sound and Vibration (2001) **241**(2), 207–222
doi:10.1006/jsvi.2000.3292, available online at http://www.idealibrary.com on IDEAL®

A THREE-DIMENSIONAL SYMMETRICAL CONDENSED TLM NODE FOR ACOUSTICS

J. A. Portí and J. A. Morente

Faculty of Sciences, Department of Applied Physics, University of Granada, 18071, *Granada, Spain.*
E-mail: jporti@goliat.ugr.es

(*Received* 7 *January* 2000, *and in final form* 17 *July* 2000)

The transmission line modelling (TLM) method is applied to acoustic problems. A three-dimensional (3-D) symmetrical condensed node for acoustics and the corresponding scattering matrix are presented. A full development of the analogy between acoustic-field quantities and pulses at the nodes is carried out that also allows the definition of excitation techniques and the imposition boundary conditions. Finally, numerical examples prove the satisfactory behaviour of the TLM method in acoustics.

1. INTRODUCTION

In the last 20 years, the transmission line modelling (TLM) method has been extensively and successfully used for the numerical simulation of electromagnetic wave propagation problems. The method substitutes a portion of an electromagnetic medium by a unitary element, termed "node". Each node comprises an appropriate set of interconnected transmission lines whose parameters (inductance and capacitance per unit length) are chosen to describe the propagation characteristics of the medium they substitute. Some of these lines allow interconnection with adjacent nodes (link or main lines), while the rest are only connected to one node and allow adjustment of the electric permittivity and magnetic permeability, i.e., the wave velocity and the impedance of the medium (stub lines). Attenuation due to the Joule effect can also be taken into account by including infinitely long stub lines at the node. In this manner, the electromagnetic wave propagation problem through a certain medium is substituted by an analogous but simpler problem of propagation and scattering of electric and current pulses inside a mesh of interconnected transmission lines [1]. The TLM method is conceptually difficult because a certain understanding of the propagation phenomenon under study and transmission line concepts is required before its application. This has probably been the main reason for which the method has not become as popular in fields outside electromagnetics as other numerical methods such as the moments method (MM) or finite differences in the time domain (FDTD), which have a more direct relationship between mathematical equations and numerical implementation, independently of the physical origin of these equations. One of the main features of the electromagnetic version of the TLM method is that charge and energy conservation conditions are included in its formulation; therefore, unless inappropriate boundary conditions are imposed, the method is intrinsically stable. However, perhaps the most outstanding advantage of TLM is that it provides a direct simulation of the phenomenon and not of the equations governing it. This feature has been

0022-460X/01/120207 + 16 $35.00/0

used to simulate efficiently the presence of special and difficult situations such as thin conducting wires [2], multi-wire systems [3] or sharp regions [4] without using the fine mesh required by other methods. Indeed, the presence of a thin wire is usually considered in FDTD as a means of imposing zero tangential electric field on the wire surface. This boundary condition requires the use of a mesh at least as fine as the wire radius, which is very expensive in memory and time calculation. As regards the TLM method, the wire can be considered not as equations, but directly as a simple transmission line circuit that can be added to the standard node defining a portion of medium much larger than the wire [2]. By means of this direct simulation, the wire can be modelled by using a very coarse mesh, which implies a considerable reduction in time calculation and memory requirements. This same concept can be easily extended to take into account the presence of multi-wire systems by simply adding an equivalent circuit for each wire [3]. The modelling of sharp conducting regions is another problematic situation in numerical methods because the fast variation of the physical quantities around these regions usually involves the use of a very fine mesh. In these regions, modified TLM nodes which carry out a direct modelling of these points allow the use of a coarse mesh without loss of accuracy [4]. It is in these critical situations in which the TLM method (by means of the inclusion of new special elements in a relatively simple and elegant form) behaves more advantageously when compared to other methods, thus justifying the growing interest concerning the TLM method in recent years [5]. The parallelism existing between different types of propagation (linear sources and sharp regions in filter design are also present in the acoustic case) seems to indicate that suitability of the TLM method for its application to problems outside the electromagnetic field.

Despite the fact that the TLM method can be applied to any phenomenon involving wave propagation, most of the works in the literature have concentrated on electromagnetic problems, with other possible applications remaining in an early stage of development. The successful application to electromagnetic phenomena seems to indicate that the same advantages will be exhibited when applied to other fields such as acoustics. In fact, simple electric-circuit models have been extensively used and can easily be found in classic books [6]. The TLM method can be considered as a more general and complicated circuit that includes spatial and temporal variables. As regards acoustic phenomena modelling with the TLM method, a few guidelines are included in reference [7], and as almost unique applications in acoustics, the TLM method is used to derive the radiation pattern of two-dimensional acoustic radiators [8], applied as a numerical tool for active noise control [9], also in a two-dimensional (2-D) case, and to study the human vocal tract [10]. As regards this last contribution, although interesting and valuable, the node it presents shows two undesirable properties when its size is different in the three Cartesian directions: first, the characteristic impedance of the link lines depends on its direction, this may produce undesired reflections between nodes, and second, the speed of pulses is equal for the three Cartesian directions in spite of the fact that the distance they must travel is different, which introduces a synchronism problem in the mesh. However, these and other applications represent important although specific contributions to the extension of the TLM method to the modelling of acoustic problems. The aim of this work is to present a more complete and unified description of most of the theoretical aspects needed for a full application of the method in acoustic problems. The plan of the paper is as follows. In section 2, a versatile three-dimensional (3-D) symmetrical condensed TLM node for acoustics is presented together with the derivation of the scattering matrix that provides the reflected pulses corresponding to a set of incident ones. Certain aspects related to analogies, excitation technique and special boundary conditions are given and discussed in section 3. Some numerical applications of different types are set out in section 4 to demonstrate the

feasibility of the TLM method for dealing with acoustic problems. The final section summarizes the main conclusions of the work.

2. AN ACOUSTIC CONDENSED NODE

The acoustic field in a fluid of equilibrium density, ρ, and coefficient of compressibility, σ, is governed by

$$\frac{\partial u_x}{\partial x} + \frac{\partial u_y}{\partial y} + \frac{\partial u_z}{\partial z} = -\sigma \frac{\partial p}{\partial t}, \qquad \frac{\partial p}{\partial x} = -\rho \frac{\partial u_x}{\partial t}, \tag{1a, b}$$

$$\frac{\partial p}{\partial y} = -\rho \frac{\partial u_y}{\partial t}, \qquad \frac{\partial p}{\partial z} = -\rho \frac{\partial u_z}{\partial t}, \tag{1c, d}$$

where p denotes dynamic pressure and u_i the ith component of the particle velocity.

Let us now consider the transmission line circuit in Figure 1(a). It is formed by the parallel connection of six transmission lines of identical characteristic admittance, $Y_0 = Z_0^{-1}$, with length $\Delta l_x/2$, $\Delta l_y/2$, and $\Delta l_z/2$, depending on its orientation. Each one of these lines defines a voltage and a current pulse travelling towards the junction from a certain Cartesian direction. An extra line, line 7, is an open-circuited or capacitive stub of characteristic admittance YY_0, which defines a voltage that is common to the rest of the lines but with no particular direction associated with it. The speed of pulses at all the lines is adjusted so that its length is covered in a fixed time $\delta t/2$. The circuit thus defines a common voltage V, with a total capacitance $C_T = Y_0(6 + Y)\delta t/2$. This circuit will be denoted the parallel node for p. It can be shown that its behaviour is controlled by the following equation:

$$\frac{\partial I_x}{\partial x} + \frac{\partial I_y}{\partial y} + \frac{\partial I_z}{\partial z} = -C_T \frac{\partial V}{\partial t}. \tag{2}$$

This equation is analogous to equation (1a) if the following equivalencies are considered:

$$p \equiv V, \qquad u_x \equiv I_x \Delta l_x, \qquad u_y = I_y \Delta l_y, \qquad u_z \equiv I_z \Delta l_z, \qquad \sigma \equiv C_T, \tag{3}$$

where I_i is a current along the i direction.

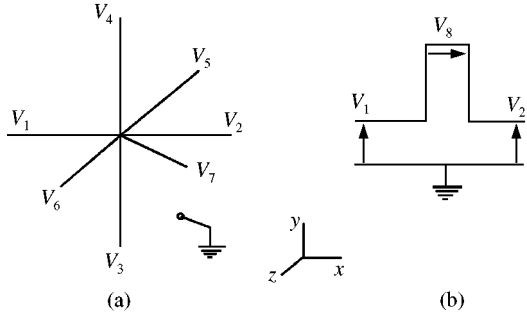

Figure 1. (a) Parallel node for p. (b) Series node for u_x.

As regards the circuit of Figure 1(b), it is formed by lines 1 and 2 of the previous circuit, both defining voltage and current I_x with propagation along the x direction. An extra short-circuited line of characteristic impedance $Z_x Z_0$ is series connected to lines 1 and 2. The length of this line is also covered in $\delta t/2$ time. This inductive stub contributes to I_x with no particular direction and adds inductance to the circuit so that the total inductance is $L_{Tx} = (2 + Z_x)Z_0\delta t/2$. The circuit defines I_x, this circuit will be termed as the series node for I_x and the differential equation that governs it is

$$\frac{\partial V}{\partial x} = -L_{Tx}\frac{\partial I_x}{\partial t}, \tag{4}$$

which is equivalent to equation (1b) provided

$$p \equiv V, \qquad u_x \equiv I_x \Delta l_x, \qquad \rho \Delta l_x^2 \equiv L_{T_x}. \tag{5}$$

Similar series nodes for I_y and I_z, involving lines 3–6 and two extra inductive stubs 9 and 10, reproduce equations (1c) and (1d). It therefore seems that the whole set of equations (1) for a cubic portion of fluid with dimensions $\Delta l_x \Delta l_y \Delta l_z$ can be described by a circuit of transmission lines resulting from combining one parallel and three series circuits. Unfortunately, these circuits are partially coupled in a way that does not allow a direct connection, i.e., a fully circuital representation. In fact, although the analogies established equations (3) and (5) are very similar, there are important differences arising from this coupling. The common voltage at the parallel node, for example, differs from the individual voltage pulses at a series node, or the common current I_x at the series node is not exactly I_x of the parallel node in Figure 1(a). Nevertheless, the basic ideas presented above are still useful to construct a 3-D node starting from a parallel node for pressure and three series nodes for the particle velocity. The main difference is that these circuits are not physically connected. Instead, formal connections governed by equations (1) are considered, resulting in the node shown in Figure 2, in which connections at the centre of the node are represented as a black box to emphasize that the connection between the circuits is not physical but formal. It is important to note that all the field quantities are defined at the same point, the centre of the node, and for this reason the node is said to

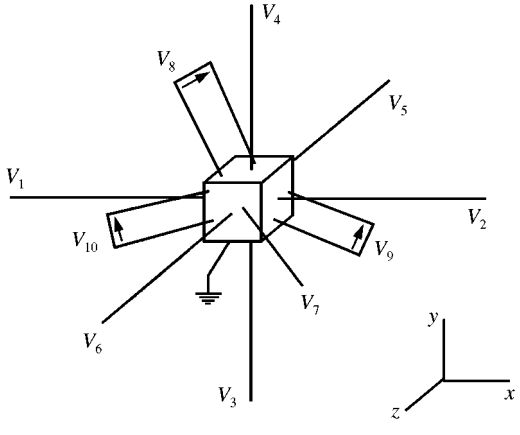

Figure 2. Acoustic symmetric condensed node.

TABLE 1

Electric–acoustic equivalencies for the acoustic node

Line	Pressure	Particle velocity	Capacitance	Inductance	Direction
1	V_1	$I_1\Delta l_x$	$Y_0\delta t/2$	$Z_0\delta t/2$	x
2	V_2	$-I_2\Delta l_x$	$Y_0\delta t/2$	$Z_0\delta t/2$	x
3	V_3	$I_3\Delta l_y$	$Y_0\delta t/2$	$Z_0\delta t/2$	y
4	V_4	$-I_4\Delta l_y$	$Y_0\delta t/2$	$Z_0\delta t/2$	y
5	V_5	$I_5\Delta l_z$	$Y_0\delta t/2$	$Z_0\delta t/2$	z
6	V_6	$-I_6\Delta l_z$	$Y_0\delta t/2$	$Z_0\delta t/2$	z
7	V_7		$YY_0\delta t/2$		
8		$I_8\Delta l_x$		$Z_xZ_0\delta t/2$	
9		$I_9\Delta l_y$		$Z_yZ_0\delta t/2$	
10		$I_{10}\Delta l_z$		$Z_zZ_0\delta t/2$	

be of the condensed type. The basic concepts of the analogy are summarized in Table 1, which shows the field quantities and direction of propagation associated with the lines, together with the capacity and inductance introduced at the node by the presence of the line.

Once the acoustic node has been defined, the TLM algorithm proceeds as follows. By means of a proper discretization of space, a mesh of transmission lines formed by interconnecting TLM nodes substitute the original medium. Time is also discretized in δt units, δt being the time needed for the voltage and current pulses to travel from the centre of the node to the centre of an adjacent node through a link line, lines 1–6, or back to the same point through a stub, lines 7–10. For time $n\delta t$ and for each node, a set of incident voltage pulses travel towards the node, reaching its centre at time $n\delta t$, scattering, and producing reflected pulses to all the lines in the node. Those pulses reflected to link lines connect to link lines of adjacent nodes, becoming incident pulses at time $(n+1)\delta t$, while pulses reflected to stubs generate incident pulses at the same node and the next time step, thus controlling the velocity of propagation.

If ${}_nV^i$ and ${}_nV^r$ stand for the column vectors containing the ordered incident and reflected pulses, these are related by

$$ {}_nV^r = \tilde{S}\,{}_nV^i, \tag{6}$$

where $\tilde{S}$ is a 10×10 matrix, termed the scattering matrix. The elements of $\tilde{S}$ are to be determined so as to contain all the information described by equations (1), together with energy conservation conditions. This procedure is usually very complicated; nevertheless, the concept of common and uncommon lines in the parallel and series nodes in Figure 1 considerably reduces the complexity of this task [11].

To obtain the first column of the scattering matrix a unique and unitary voltage pulse, $V_1^i = 1$, travelling towards the centre of the node through line 1, is considered. This line defines p and u_x propagating along the x direction. These magnitudes appear in equations (1a) and (1b), i.e., in the parallel circuit for p, and the series circuit for I_x. From these circuits, pulses reflected to all their lines may appear. Let the amplitude of these reflected pulses be $V_1^r = a_x$, $V_2^r = b_x$, $V_3^r = V_4^r = V_5^r = V_6^r = c$, $V_7^r = d$, and $V_8^r = -e_x$. Considering incident pulses for all the lines in the node, the following initial form of the scattering matrix

can be obtained

	1	2	3	4	5	6	7	8	9	10
1	a_x	b_x	c	c	c	c	f	$-h_x$		
2	b_x	a_x	c	c	c	c	f	h_x		
3	c	c	a_y	b_y	c	c	f		$-h_y$	
4	c	c	b_y	a_y	c	c	f		h_y	
5	c	c	c	c	a_z	b_z	f			$-h_z$
6	c	c	c	c	b_z	a_z	f			h_z
7	d	d	d	d	d	d	g			
8	$-e_x$	e_x						j_x		
9			$-e_y$	e_y					j_y	
10					$-e_z$	e_z				j_z

(7)

To obtain the explicit values for the parameters appearing in $\tilde{S}$, consider again the unitary pulse through line 1 which produces pulses reflected to lines 1–7 with amplitudes given by the first column of matrix (7). All the lines except 1 and 2 appear in the series or in the parallel circuit but not in both circuits; these are the uncommon lines. Information about these lines is only contained in one of the circuits in Figure 1, with no formal coupling, so the coefficients c, d, and e_x can be easily calculated from the transmission coefficient for the corresponding circuit. By doing so,

$$c = d = \frac{2}{6 + Y}, \qquad e_x = \frac{2Z_x}{2 + Z_x}. \tag{8}$$

As regards lines 1 and 2, they are common to both circuits so the parameters a_x and b_x cannot be obtained directly from one circuit or the other because there is some degree of coupling between them. Instead, these will be directly calculated from equations (1a) and (1b), which are the actual origin of this coupling, and Table 1. A first order approximation for equation (1a) is

$$\frac{\Delta l_x(-I_2) - \Delta l_x I_1}{\Delta l_x} + \frac{\Delta l_y(-I_4) - \Delta l_y I_3}{\Delta l_y} + \frac{\Delta l_z(-I_6) - \Delta l_z I_5}{\Delta l_z} = -C_T \frac{\partial V}{\partial t} \tag{9}$$

from which

$$\sum_{i=1}^{6} I_i = \frac{\partial Q_T}{\partial t}. \tag{10}$$

To evaluate the derivative of the total charge Q_T stored at the node through the capacitive stub, it must be noted that in $\delta t/2$ the incident pulses turn into reflected pulses. Therefore, in this $\delta t/2$ time, the charge at the stub changes from an initial value proportional to capacitance of the line and the incident voltage pulse to a final value proportional to the capacitance and the reflected pulse. Concretely,

$$\frac{\partial Q_T}{\partial t} = \frac{Y_0 Y \delta t/2 (V_7^r - V_7^i)}{\delta t/2} = Y_0 Y (V_7^r - V_7^i) = -I_7. \tag{11}$$

So, from equations (10) and (11), the coupling condition imposed by equation (1a) is the following charge-conservation condition at the parallel node:

$$\sum_{i=1}^{7} I_i = 0. \tag{12}$$

By a similar procedure involving equation (1b), it can be shown that the following continuity of potential condition must also be met:

$$V_1 - V_2 + V_8 = 0. \tag{13}$$

Equations (12) and (13) represent two additional conditions from which parameters a_x and b_x can be easily obtained. By doing so,

$$a_x = \frac{1}{2}\frac{Z_x - 2}{Z_x + 2} - \frac{1}{2}\frac{Y + 2}{Y + 6}, \qquad b_x = -\frac{1}{2}\frac{Z_x - 2}{Z_x + 2} - \frac{1}{2}\frac{Y + 2}{Y + 6}. \tag{14}$$

The values corresponding to columns 2–6 of the scattering matrix are analogous to the values given by equations (8) and (14) if the appropriate value of the relative characteristic impedance is chosen. Finally, applying this procedure to pulses incident from the stubs yields

$$f = \frac{2Y}{Y + 6}, \qquad g = \frac{Y - 6}{Y + 6}, \qquad h = \frac{2}{Z + 2}, \qquad j = \frac{2 - Z}{2 + Z}, \tag{15}$$

where it is understood that the appropriate subscript for Z is taken for the last two parameters.

3. EQUIVALENCES AND RELATED TOPICS

In this section, some aspects about the choice of the node parameters are presented and discussed. Precise expressions that define field quantities starting from voltage or current pulses are also obtained and a discussion about how to impose a certain external field and special boundary conditions are also considered.

3.1. GENERAL RELATIONSHIPS

Equations (3) and (5) relate the equilibrium density and coefficient of compressibility to the total capacitance and inductance of the node. So, for a certain fluid, the following expression is met:

$$\sigma = \frac{Y_0 \delta t}{2}(6 + Y), \qquad \rho = \frac{Z_0 \delta t}{2}\frac{(2 + Z)}{\Delta l^2}. \tag{16}$$

It must be noted that the equation for ρ holds for all the Cartesian directions, so Z and Δl can take coherent subscript, x, y, or z. From the above equations, the relative admittance and characteristic impedances are easily obtained. In addition, the group velocity and acoustic impedance of the modelled medium at low frequencies are given by

$$v_g = \frac{2v_l}{\sqrt{(6 + Y)(2 + Z)}}, \qquad Z_{AC} = \frac{Z_0}{\Delta l}\sqrt{\frac{2 + Z}{6 + Y}}, \tag{17}$$

where v_l, Z, and Δl can take the subscripts x, y, and z, v_l being the speed of voltage pulses at a given line.

From the above equations it becomes clear that the value of Z_0 is not really relevant since the parameters Y and Z are enough to define appropriate values for group velocity and acoustic impedance. Nevertheless, a judicious choice may simplify some expressions. Concretely, the following value will be chosen:

$$Z_0 = Y_0^{-1} = Z_{AC}\sqrt{3}h, \tag{18}$$

where h is $\min\{\Delta l_x, \Delta l_y, \Delta l_z\}$. With this choice there is no need for using stubs at all for an isotropic medium when the node size is identical in all Cartesian directions and the time step takes its maximum allowable value of

$$\delta t = \frac{h}{v_g\sqrt{3}}. \tag{19}$$

In addition, for isotropic inhomogeneous media, the use of the capacitive stub alone allows ρ and σ to be determined, while conversely, the inductive stubs alone are able to control the main characteristics if the medium shows anisotropic properties.

To obtain the relationship between the voltage pulses and field quantities, the common voltage at the parallel node in Figure 1(a) and the common current at the series nodes in Figure 1(b) must be calculated. Thevenin's equivalent circuit from the junction terminals for a given line with incident and reflected pulses is a series connection of its characteristic impedance and twice the incident voltage pulse [7]. Thus, the need for reflected pulses is avoided and the relations are simpler. Thevenin's theorem for the nodes in Figure 1 for p and I_x yields the circuits in Figure 3, from which the following expressions for the pressure field and particle velocity in the x direction can be obtained:

$$p \equiv V = \frac{2}{6+Y}\left\{\sum_{j=1}^{6} V_j^i + YV_7^i\right\}, \qquad u_x \equiv \Delta l_x I_x = \frac{\Delta l_x(V_1^i - V_2^i + V_8^i)}{Z_0(1 + Z_x/2)}. \tag{20}$$

Similar results are directly derived for u_y and u_z.

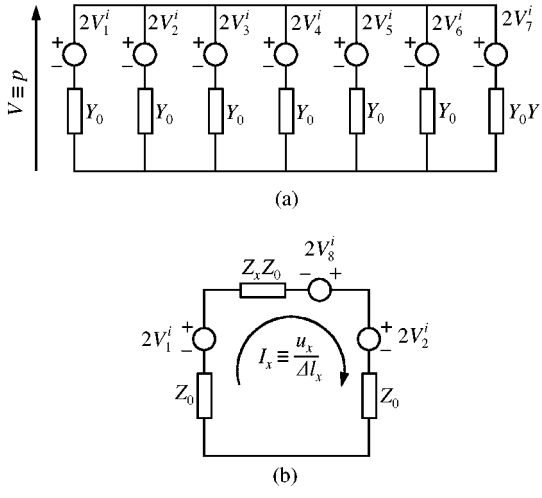

Figure 3. Equivalent circuits for p and u_x.

3.2. EXCITATION TECHNIQUE

A direct consequence of equation (20) is that voltage pulses needed to impose a given acoustic field p_0, $\mathbf{u}_0$ are

$$V_{1,2} = \frac{p_0}{2} \pm \frac{Z_0 u_{0x}}{2\Delta l_x}, \qquad V_{3,4} = \frac{p_0}{2} \pm \frac{Z_0 u_{0y}}{2\Delta l_y}, \qquad V_{5,6} = \frac{p_0}{2} \pm \frac{Z_0 u_{0z}}{2\Delta l_z}, \qquad V_7 = \frac{p_0}{2},$$

$$V_8 = \frac{u_{0x} Z_x Z_0}{2\Delta l_x}, \qquad V_9 = \frac{u_{0y} Z_y Z_0}{2\Delta l_y}, \qquad V_{10} = \frac{u_{0z} Z_z Z_0}{2\Delta l_z}. \tag{21}$$

These equations yield voltage pulses that can be added at each time step to pulses already existing in the TLM mesh, thus providing a way to excite a desired acoustic field. However, some usual but particular cases can be considered regarding the excitation technique.

The first case to consider is the presence of a rigid piston that vibrates with a certain velocity $u_0(t)$. The geometry for an x-oriented piston between two nodes is shown in Figure 4(a). The piston connects to link line 1 of node (i, j, k) and to line 2 of the node $(i-1, j, k)$. Considering only the right side, at time $n\delta t$, a reflected pulse ${}_nV_1^r$ travels towards the piston. As the piston effect is fixing the velocity and this acoustic quantity is related to current, the piston can be electrically modelled by a current source $i(t) = u_0(t)/\Delta l_x$. Figure 4(b) is the equivalent circuit for the situation at the moment the reflected pulse reaches the piston, time $(n + \frac{1}{2})\delta t$. From this circuit it can be seen that

$${}_{n+1/2}V_1 = {}_nV_1^r + {}_{n+1}V_1^i = 2{}_nV_1^r + \frac{u_0((n+1/2)\delta t)}{\Delta l_x} Z_0 \tag{22}$$

from which the incident pulse at the next time step can be obtained.

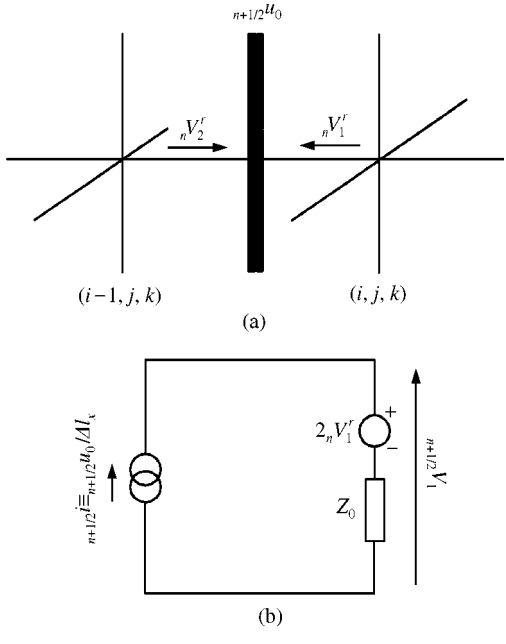

Figure 4. (a) x-oriented piston. (b) Equivalent circuit.

A case similar to a piston is that of a source that fixes a certain pressure $p_0(t)$. The equivalent circuit is similar to that of Figure 4(b), with the current source substituted by a voltage source $v(t) = p_0(t)$. The equation allowing the incident pulse at $n + 1$ time step to be obtained is now

$$ {}_{n+1/2}V_1 = {}_nV_1^r + {}_{n+1}V_1^i = p_0((n + 1/2)\delta t). \tag{23} $$

The final situation of interest is that in which sources are so far away that their simulation would require an extremely large mesh. This is the case, for example, of a plane wave propagating towards a certain scatterer. The incident wave is perfectly known and described by means of analytical functions for pressure and particle velocity. In these cases, it is useful to define a closed imaginary surface whose limits are halfway between nodes and with all the scattering objects inside the region it defines. The incident field is calculated at intermediate time steps over the imaginary surface. The corresponding voltage pulses are then calculated from equation (21), being added to the existing pulses of adjacent lines entering the closed surface and subtracted from existing pulses of adjacent lines outside this region [12]. In this manner, the imaginary surface is transparent to the scattered field but imposes the extra incident field so as to let the total field propagate inside the inner region while allowing only the scattered field to escape from the closed surface.

To illustrate the above discussion, consider, for instance, a portion of the whole closed surface that is plane and oriented normal to the x direction, halfway between nodes (i, j, k) and $(i + 1, j, k)$. If, for a certain time, $(n + \frac{1}{2})\delta t$, the incident field at the interface is given by $p_0(t)$ and $u_{0x}(t)$, the incident pulses at time step $n + 1$ are

$$ \begin{aligned} {}_{n+1}V_1^i(i + 1, j, k) &= {}_nV_2^r(i, j, k) + \left(\frac{p_0((n + 1/2)\delta t)}{2} + \frac{Z_0 u_{0x}((n + 1/2)\delta t)}{2\Delta l_x}\right), \\ {}_{n+1}V_2^i(i, j, k) &= {}_nV_1^r(i + 1, j, k) - \left(\frac{p_0((n + 1/2)\delta t)}{2} - \frac{Z_0 u_{0x}((n + 1/2)\delta t)}{2\Delta l_x}\right). \end{aligned} \tag{24} $$

3.3. BOUNDARY CONDITIONS

The modelling of objects or special conditions in the medium can be taken into account in different ways. The most direct form is to introduce the element as a specific boundary condition on pressure, particle velocity or as a combination of both. This is done by simply substituting the presence of an object by its acoustical impedance. In spite of its simplicity, this method provides accurate results for a great number of problems. It must be noted that the acoustic impedance is a pressure divided by a particle velocity; however, only electrical impedance must be considered in the TLM mesh. According to the analogy summarized in Table 1, this means that a given acoustic impedance normal to a certain direction corresponds to an electrical impedance in the TLM mesh that equals the acoustic impedance multiplied by the node size in that particular direction.

Now suppose that a certain node (i, j, k) is located at the right side of a certain object which can be modelled by means of an acoustic impedance Z_A. At time $(n + \frac{1}{2})\delta t$, a reflected pulse ${}_nV_1^r(i, j, k)$ reaches the object from the node. Thevenin's theorem allows an equivalent circuit formed with a voltage source $2{}_nV_1^r(i, j, k)$ feeding a series connection of Z_0 and $Z_A\Delta l_x$ to be defined. It is then straightforward to obtain the total voltage at the line from which the following incident pulse is obtained:

$$ {}_{n+1}V_1^i(i, j, k) = {}_nV_1^r(i, j, k)\left(\frac{Z_A\Delta l_x - Z_0}{Z_A\Delta l_x + Z_0}\right). \tag{25} $$

In the particular case of a perfectly rigid wall, the acoustic impedance is ∞ and the pulse reflects, maintaining amplitude and sign.

The problem of modelling infinite-size media is carried out by introducing an artificial truncation of the TLM mesh as close as possible to the objects that scatter the acoustic field. The eliminated medium is substituted by appropriate absorbing boundary conditions (ABCs) which must eliminate the artificial reflection that would occur at the truncated limits. As regards electromagnetic applications, the most usual conditions include matching of the mesh by substituting the truncated medium by its electromagnetic impedance or TLM adaptations of conditions usually used in the FDTD method [13]. These conditions provide satisfactory results for certain angles, but important reflections may appear for other orientations. In recent years, conditions based on introducing a special dissipative medium that separates components of the field (perfectly matched layer), produce almost negligible reflection for all incidence angles [14]. A complete study of the behaviour of different ABCs in acoustic applications is beyond the scope of this work, so, for the moment, the ABCs used in the numerical applications presented in the next section will use the natural matching way that the TLM suggests, i.e., equation (25) with an electrical load of value of

$$Z_L = \frac{Z_A \Delta l}{\cos \phi}, \tag{26}$$

where Z_A stands for the acoustic impedance of the eliminated medium, Δl is the node length in the normal to the boundary–surface direction, and ϕ is the incident angle. With the inclusion of the angle, which be calculated for any node at the boundary, the results are quite satisfactory unless a dispersive medium is considered, since in this case each frequency has its own incident angle. Figure 5 shows the reflection coefficient versus frequency for normal and 45° incidence. In both cases, the reflection coefficient is below -20 dB for normalized frequencies ranging from zero to $\Delta l/\lambda = 0{\cdot}1$. This is fairly a good result for such a simple condition, comparable to other results obtained with more elaborate conditions [15]. The explanation for the poorer reflection coefficient for frequencies above the normalized frequency value 0·1 is not due to the ABC but due to the numerical dispersion introduced by the discrete mesh. A comparative study of the dispersion introduced by the spatial discretization in the TLM and FDTD methods for electromagnetic applications shows that both methods introduce similar numerical errors due to numerical dispersion

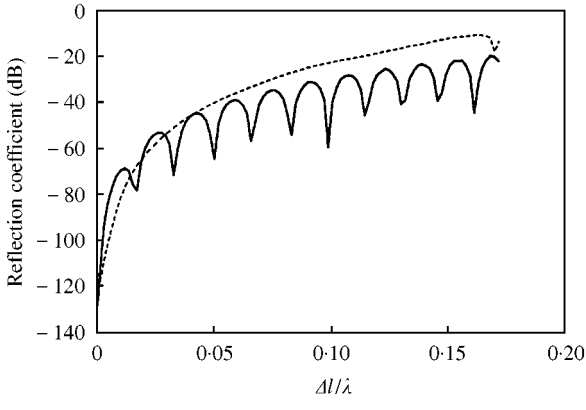

Figure 5. Reflection coefficient for normal and 45° incidence: —— normal incidence; - - - - 45° incidence.

[16]. This unavoidable erroneous behaviour increases with the frequency, thus introducing a limiting upper frequency for the valid results. In normalized terms, this upper frequency is $\Delta l/\lambda = 0{\cdot}1$ [16], which is in good agreement with the acoustic results shown in Figure 5.

4. NUMERICAL RESULTS

To demonstrate the applicability of the acoustic node and the considerations discussed in the previous sections, different practical problems are solved. The first example consists in determining the resonant frequencies for a cubic box filled with air. The box is limited by rigid walls with lengths (20 cm, 30 m, 40 m) and is modelled with a mesh of symmetrical nodes of equal direction in all Cartesian directions, $\Delta l = 2$ cm, maximum allowable time step, $\delta t = 3{\cdot}48853 \times 10^{-5}$ s, with no capacitive nor inductive stub. Taking 331 m/s as the speed of sound in air, this node size and the limit imposed by numerical dispersion, the maximum valid frequency is slightly above 1·6 kHz. A delta pulse is added to all the lines of the node located at point (1, 1, 1) and the output pressure is taken at point (9, 14, 19). The excitation and output points are taken near walls to avoid points where a certain mode may vanish. Ten thousand time calculations have been carried out for the Fourier transform to give a frequency precision slightly below 3 Hz. The total CPU time needed to carry out this calculation on a Pentium II at 350 MHz has been 36 s.

Figure 6 is a plot of the numerical output pressure versus frequency in which resonances are clearly appreciated, while Table 2 is a comparison of theoretical and TLM resonant frequencies for some low-frequency modes. Good agreement is observed for all the modes below the above-mentioned limiting frequency.

To test the effect of stubs, the same cavity has been modelled with a mesh of nodes of different size in each Cartesian direction. In this case, the node size is (2, 3, 4 cm). With this choice, the cavity is (10, 10, 10) in node units, the maximum valid frequency is now lower than in the previous example, slightly above 820 Hz. Ten thousand calculations have been carried out requiring a CPU time of 20 s. The resonant frequencies and relative error of modes below this limiting value are presented in the last two columns of Table 2. Results are also satisfactory for frequencies below the upper limit mentioned above. Even for modes above 820 Hz, such as modes 020 and 112, errors are quite acceptable.

Finally, consider an open example in which special excitation technique and boundary conditions are required. The problem is the long rectangular duct loaded with a cubic

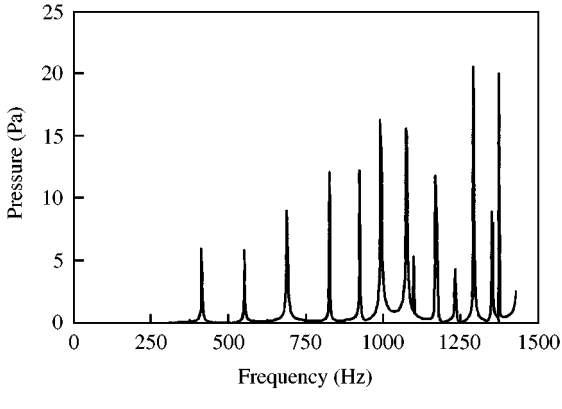

Figure 6. Output pressure versus frequency for the rectangular cavity of dimensions (20, 30, 40 cm). The TLM node size is (2, 2, 2 cm).

TABLE 2

Resonant frequencies in Hz for the rectangular cavity of dimensions (20, 30, 40 *cm*)

Mode	Theory	TLM mesh (2, 2, 2 cm)	Error (%)	TLM mesh (2, 3, 4 cm)	Error (%)
001	413·8	412·8	0·24	415·7	0·46
010	551·7	550·4	0·24	553·2	0·27
011	689·6	688·0	0·23	688·8	0·12
002–100	827·5	825·6	0·23	825·6	0·23
101	925·2	923·0	0·24	923·0	0·24
012	994·5	991·8	0·27	991·8	0·27
020	1103·3	1097·9	0·51	1109·4	0·55
112	1292·8	1292·8	0·0	1287·1	0·44

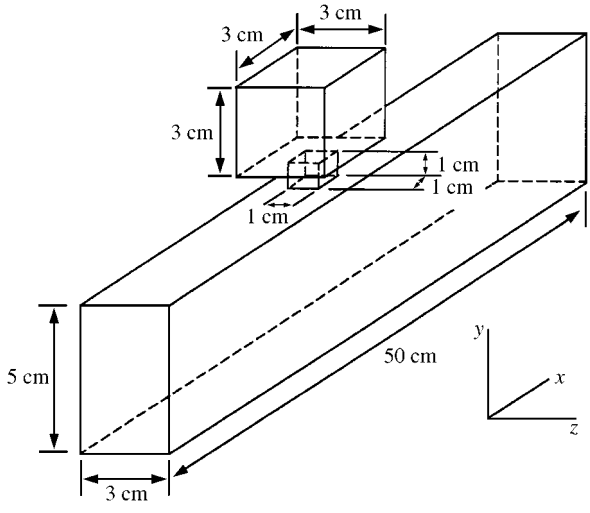

Figure 7. Long duct loaded with a Helmholtz resonator.

Helmholtz resonator at the top (Figure 7). A fairly good approximation for the resonant frequency of the Helmholtz resonator is obtained by considering an analogous electric circuit formed by the series connection of a capacitor and an inductor [17]. This zero-dimensional model provides the following approximated value for the resonant frequency:

$$f_r = \frac{c}{2\pi}\sqrt{\frac{S}{VL'}}, \tag{27}$$

where V is the cavity volume of the resonator, S the neck area, and L' effective length. This effective length takes into account the volume of air near the neck and for our example it is $L' = L + 1{\cdot}7a$, where a is the radius of a circular neck of equal area [17]. The resonator side is 3 cm long in all directions and the neck is 1 cm long with a square hole of side 1 cm located at the centre of a side. With these values $V = 27$ cm^3, $S = 1$ cm^2, and $L' = 1{\cdot}959$ cm, therefore the theoretical value for the resonant frequency given by equation (27) is 724·3 Hz. The dimensions of the duct are 50, 5, and 3 cm in the x-, y-, and z-Cartesian directions

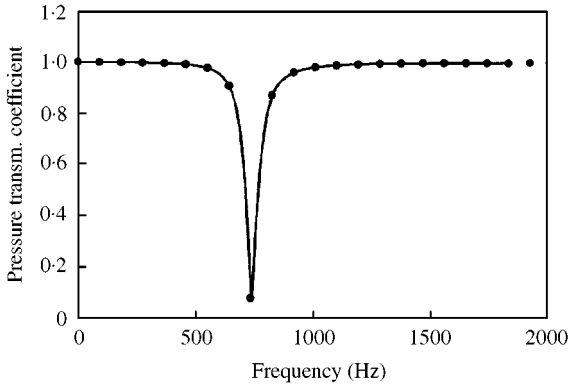

Figure 8. Pressure transmission coefficient versus frequency for the long duct with Helmholtz resonator: —— TLM; –●– FDTD.

respectively. The system is modelled with a mesh of condensed nodes of equal size in the three Cartesian directions, $\Delta l = 0{\cdot}25$ cm, using the maximum time step, $\delta t = 4{\cdot}36065 \times 10^{-6}$ s. This value of Δl ensures valid results slightly above 13 kHz. The mesh dimensions are (200, 36, 12) in Δl units. A Gaussian pulse is used to excite the fundamental mode at an x-plane located at $x = 5$ with a time constant of 13 000/s which corresponds to a bandwidth of 6·5 kHz. For the considered field, propagation takes place along the axis of the ducts for all frequencies, so matching ABCs based on equation (26) are used with $\phi = 0$. Figure 8 shows the pressure transmission coefficient obtained with the TLM method. As expected, the Helmholtz resonator eliminates the propagation at frequencies near the resonance. The numerical value corresponds to 733·8 Hz, which is in close agreement with the theoretical value provided by equation (27). An independent finite-differences solution is also included for comparison. The total CPU time needed to carry out 10 000 TLM calculations in this large mesh has been 19 min 20 s, while the time required for the FDTD calculation has been slightly lower, 16 min 50 s. This small difference between both calculations is surprising. Effectively, the FDTD scheme calculates only four quantities while the TLM algorithm, at least, determines six voltage pulses, 1·5 times the FDTD requirement. This factor seems to indicate that the calculation time using the TLM method must be 1·5 times the FDTD one. This is basically true in a simple situation such as the one presented in the first example where, as indicated, the time required by the TLM algorithm was 36 s, while the FDTD method spent only 25 s for the same mesh. With regard to the second example, the imposition of rigid boundaries is more direct in the TLM method, thus reducing the expected difference in the CPU time. It is worth noting that this extra information provided by the TLM method, the total field quantities at the centre of the node and some of these quantities at points halfway between nodes, adds versatility to the method when imposing the presence of rigid or other types of boundaries, not only halfway between nodes but also at their centre. In fact, the problems considered in this section have been chosen so that each rigid boundary is located exactly between nodes, but in general, boundaries will be placed at arbitrary points and this extra possibility for locating boundaries is very useful for considering these problems without the need of extra interpolations. Finally, it is interesting to note that using a fine mesh not in the whole problem, but only at points near the resonator neck, where rapid field variations are present, may considerably reduce the computation time.

5. CONCLUSIONS

A 3-D symmetrical condensed TLM node for the modelling of acoustic problems has been presented in this paper. The node is a formal connection of individual transmission line circuits that shows interesting properties such as symmetry, versatility to model different situations, definition of field quantities at a unique point, etc. The scattering matrix has been obtained by using the concept of common and uncommon lines for coupled circuits. These circuits are also useful to define the quantities involved in the acoustic-electric analogy, and the results are applied to describe the excitation technique and the presence of special conditions. Finally, numerical examples demonstrate the capability of the TLM method for dealing with acoustic phenomena with an accuracy similar to that obtained with other methods such as FDTD. The favourable behaviour demonstrated by the TLM method when applied to specially difficult electromagnetic problems (also present in the acoustic case), together with the versatile properties that the inclusion of stubs provides the presented 3-D acoustic node, seems to be a starting point for the numerical simulation of acoustic problems from a different and promising point of view.

ACKNOWLEDGMENT

The authors would like to thank the referees for their valuable comments that have produced an optimization in the computation time, and Miss Christine M. Laurin for her help in preparing this manuscript.

REFERENCES

1. P. B. JOHNS 1986 *IEEE Transactions on Microwave Theory and Techniques* **35**, 370–377. A symmetrical condensed node for the TLM method.
2. J. A. PORTÍ, J. A. MORENTE, M. KHALLADI and A. GALLEGO 1992 *Electronic Letters* **28**, 1910–1911. Comparison of thin-wire models for the TLM method.
3. A. J. WLODARCYCK, V. TRENKIC, R. SCARAMUZA and C. CHRISTOPOULOS 1998 *IEEE Transactions on Microwave Theory and Techniques* **46**, 2431–2437. A fully integrated multiconductor model for TLM.
4. J. A. PORTÍ, J. A. MORENTE, H. MAGÁN and O. TORRES 1999 *Applied Computational Electromagnetics Society Journal* **14**, 67–71. Improved modelling of sharp zones in resonant problems with the TLM method.
5. M. NEY, P. SAGUET and D. POMPEI (Workshop Directors) *Digest of the Third International Workshop on Transmission Line Matrix* (*TLM*), *Nice* 1999.
6. L. L. BERANEK 1954 *Acoustics*. New York: McGraw-Hill.
7. C. CHRISTOPOULOS 1995 *The Transmission-Line Modelling Method*: *TLM*. Oxford: IEEE and Oxford University Press.
8. A. H. M. SALEH and P. BLANCHFIELD 1990 *International Journal of Numerical Modelling* **3**, 39–56. Analysis of acoustic radiation patterns of array transducers using the TLM method.
9. W. O'CONNOR and F. CAVANAGH 1997 *Applied Acoustics* **50**, 247–255. Transmission line matrix acoustic modelling on a PC.
10. S. EL-MASRI, X. PELORSON, P. SAGUET and P. BADIN 1998 *International Journal of Numerical Modelling* **11**, 133–151. Development of the transmission line matrix method in acoustic applications to higher modes in the vocal tract and other complex ducts.
11. J. A. PORTÍ, J. A. MORENTE and M. C. CARRIÓN 1998 *Electronics Letters* **34**, 1763–1764. Simple derivation of scattering matrix for TLM nodes.
12. F. J. GERMAN 1994 *Electronics Letters* **30**, 689–690. General electromagnetic scattering analysis by the TLM method.
13. J. A. MORENTE, J. A. PORTÍ and M. KHALLADI 1992 *IEEE Transaction, on Microwave Theory and Techniques* **40**, 2095–2099. Absorbing boundary conditions for the TLM method.

14. J. P. BERENGER 1994 *Journal of Computational Physics* **114**, 185–200. A perfectly matched layer for the absorption of electromagnetic waves.
15. J. B. SCHNEIDER and O. RAMAHI 1998 *Journal of the Acoustical Society of America* **104**, 686–693. The complementary operators method applied to acoustic finite-difference time-domain simulations.
16. J. A MORENTE, G. GIMÉNEZ, J. A. PORTÍ and M. KHALLADI 1995 *IEEE Transaction on Microwave Theory and Techniques* **42**, 514–517. Group and phase velocities in the TLM-symmetrical-condensed node mesh.
17. L. E. KINSLER, A. R. FREY, A. B. COPPENS and J. V. SANDERS 1982 *Fundamentals of Acoustics*. New York: Wiley.